Influence of polycrystalline material on crater shape optimization and roughness using low-power/low-pressure direct-current glow discharge mass spectrometry

Gagan Paudel*[a], Sergey Khromov[a], Martin Kasik[b], Hans Jørgen Roven[a] and Marisa Di Sabatino[a]

Depth profiling is an attractive approach for analysis of non-homogeneous samples and layered materials. This application requires an optimum sputtered crater profile, which means a flat crater bottom with steep walls and a low roughness. It is known that discharge parameters are one of the most important factors influencing the crater shape. Hence, in the present work, different combinations of GDMS discharge current, voltage and argon flow, giving a flat crater bottom in tantalum are presented. A combination of mechanical profilometry, scanning electron microscopy and electron back scattered diffraction is used to show the contribution of grain orientation on various sputtering characteristics and crater bottom roughness. The results of the study indicate that differential sputtering is consistent at both higher and lower discharge conditions. The crater bottom roughness can be attributed to the differential sputtering of grains in polycrystalline materials.

A. Introduction

The glow discharge mass spectrometry (GDMS) utilizes glow discharge plasma to sputter atoms from the sample surface. Hence, atoms translate to ions that constitute the plasma. The ions thus formed are separated based on differences in their mass to charge ratio, allowing multi-elemental characterization. In general, GDMS offers two major applications namely bulk analysis and depth profiling.[1-3] For bulk analysis, as impurities are considered to be sufficiently homogenous throughout the sample, specific concentration of each element/isotope is usually obtained after a pre-sputtering when a steady glow discharge is reached. The bulk analysis is applied in quality assessment of metals, alloys, polymers, semiconductors, insulators etc.[3, 4] The flat shaped samples allow characterization of concentration changes of analytes as a function of depth, i.e. depth profiling. Depth profiling has been used to determine coating performance, quality control related to elemental diffusion etc. The method can be used to profile coatings,[5] films,[6] bi- and multilayered materials.[7, 8] It should be mentioned that secondary ion mass spectrometry (SIMS) can be used for depth profile analysis with better depth and lateral resolution.[9] Nevertheless, SIMS is often compromised by limited availability of matrix-matched standards. Besides SIMS, other techniques such as X-ray photoelectron spectroscopy (XPS) and Auger electron spectroscopy (AES) can discriminate the crater edge effects by analyzing inner part of sputtered crater. In these analytical techniques, sputtering is more time consuming. Also mixing effects are stronger leading to matrix related effect. GDMS is less matrix dependent due to separation of sputtering and ionization events in space and time. Hence, GDMS is less affected by limited availability of matrix-matched standards. Another well-established analytical technique used for depth profiling is glow discharge optical emission spectroscopy (GDOES).[2, 10] In 2017, Lobo et al. reviewed depth profiling applications of both GDMS and GDOES.[11] Comparatively, GDOES is more popular than GDMS for depth profiling and quality control applications in various industries. However, GDOES is limited to detection of impurities in percentage to parts per million (ppm) level. GDMS, however, offers dynamic range detection comprising up to 12 orders of magnitude, i.e. from percentage to parts per billion (ppb).[12, 13] Thus, due to analytical merits of GDMS there is a need to improve its depth profiling capabilities.

Depth profiling relies on the assumption that atoms in the sample surface are eroded layer by layer, thus allowing conversion of time related- to depth related information. Therefore, for depth profiling a flat crater is a pre-requisite to ensure that atoms are sputtered from the same depth (layer) at a given time and hence ionized and recorded simultaneously. However, non-uniform sputtering is commonly encountered. It has been demonstrated by Bogaerts and Gijbels that the electric potential distribution in front of the sample is slightly curved at the proximity of the anode front plate aperture as compared to the center of the sample.[14] This leads to enhanced influx of energetic argon ions towards the edge of the front plate anode aperture, leading to more sputtering at edges as compared to the sample center. This phenomenon is referred to as an edge effect (also named trenching). Bogaerts et al. developed the work further and suggested that the electric potential distribution in front of the cathode can be modified by changing current and voltage to mitigate the edge effect.[15] In general, keeping the current constant while voltage is increased, the crater profile changes from concave (U-shaped crater) to convex (W-shaped crater).[15] Thus, combinations of current and voltage that lead to flat craters can be determined empirically. Optimal combinations of these two parameters depend on the instrument, specimen matrix, type of discharge gas and flow rates (pressure). Work along these lines has been performed for low-power/low-pressure GDMS with mega cell

design (VG9000, Thermo Scientific)[14] and with fast-flow/high-pressure GDMS with Grimm-type GD cell geometry (Element GD, Thermo).[16] Another instrument that relies in continuous direct current, Astrum (Nu Instruments, UK) is also a low-power/low-pressure GDMS like VG 9000. However, a systematic work demonstrating a crater shape optimization is missing for analysis with Astrum GDMS. Hence, this instrument is used in the presented study.

Moreover, Demény et al. demonstrated that the electrical field distribution of a glow discharge lamp can be modified by changing the anode tube geometry.[17] Such modifications in geometry resulted into change in crater shapes of steel sample due changes in sputtering rates. For Astrum, the entire GD cell body acts as anode which is not modified in the present study.

Furthermore, non-homogenous temperature distribution is often encountered in a crater.[18] High sample surface temperature may lead to matrix evaporation for some materials with a high vapor pressure such as zinc.[19] Therefore, GDMS users/operators during sputtering process look for approaches so that likelihood of sample heating can be reduced. One of such possibilities is to use pulsed glow discharge (PGD) source instead of continuous GD source so that the sample thermal stress is reduced. Likewise, another approach is to use instruments that offer cryocooling, such as Astrum and VG 9000. In that case, the sample heating during sputtering can be compensated.

Further, Ferreira and Büger demonstrated copper redeposition during a sputtering process using a glow discharge lamp through copper ion micrographs, which were generated from an ion microprobe mass analyser.[20] It should be noted that these authors also sputtered redeposited material. After a short period of time an equilibrium between simultaneously occurring events of sputtering and redeposition was occurring. The rate and amount of deposition and re-sputtering also change with the discharge current and voltage used, which ultimately contributes to the final crater shape.

Another important aspect of crater shape is steepness of the crater wall. The ideal crater walls would be perpendicular to the sample surface. However, sloped walls are commonly observed as incoming and outgoing species are deflected at and around the edge of the anode front plate aperture. Raith et al. demonstrated that use of high purity tantalum metal masks with an aperture smaller than the anode aperture could improve the crater wall steepness.[21] Also, the work of Bogaerts and Gijbels had a similar recommendation.[14] However, an instrument operator should be aware that use of masks may lead to higher blank values. This could prohibit use of masks, for example when analyzing materials such as high purity silicon. Therefore, deployment of masks is not considered in the presented study.

The Astrum GDMS is one of the latest commercial developments. The present authors are not aware of any journal publication demonstrating work on crater shape optimization using this instrument. However, during the European glow discharge symposium 2018, Disch presented some examples of optimum crater profiles for a copper matrix using Astrum GDMS.[22] Later, it was proposed that voltage (in kV) to current (in mA) ratio in range of 0.3-0.4 (kV/mA) leads to flat craters. In the present work, discharge parameters that lead to flat craters in tantalum are investigated. Hence, the current to voltage ratio giving an optimum crater for tantalum is proposed. Moreover, it is commonly observed among GDMS users that sputtering often leads to more surface roughness at the bottom of the crater. In the current work, we investigate and discuss the factors that can cause this effect with focus on the material`s grain orientation. Specifically, the effect of grain orientation on differential sputtering is clearly demonstrated.

B. Experimental

Sample preparation and Method

Two sets of tantalums were used in the present study - one with large irregular grains larger than 1 mm in size and another with regular grains less than 1 mm. For simplicity the former group is referred to as a test sample while the latter is denoted a control sample. All tantalum samples were grinded by grit 800 SiC paper, rinsed with water and ethanol. The samples were dried using hot gun air before being inserted into the instrument (Astrum, Nu Instruments, UK). This instrument has a low-pressure ion source, double focusing mass analysers and a dual detector system. For the present work, a flat cell GD design using a flat sample holder with 10 mm tantalum front plate orifice was used that resulted into the crater diameter of 10 mm. The specimens were cryogenically cooled for about 15 minutes before sputtering. A constant current mode was deployed to control and stabilize glow discharge conditions. High purity (6N) argon was used as a discharge gas. After sputtering the crater profile was measured mechanically by a profilometer (MarSurf M 400, Mahr GmbH Göttingen, Germany). The obtained crater was then studied by field emission scanning electron microscopy (SEM, Zeiss Ultra 55, Jena, Germany) and electron

back scatter diffraction (EBSD, NORDIF UF-1100 detector, Trondheim, Norway). For SEM, the primary electron beam was accelerated with voltage of 20 kV and an objective aperture lens of 30 µm was selected. The obtained secondary electrons from the specimen were detected using a secondary electron detector. For EBSD, the sample was tilted at 70° before being probed by the primary electron beam accelerated with energy of 20 kV. The 300 µm objective aperture lens was selected. The working distance (WD) was ~ 25 mm. Appropriate adjustments were made to compensate for the tilt angle such that the sample was brought to focus before recording the Kikuchi patterns using an EBSD detector. All EBSD scans were taken with the same area size of 225*255 µm and 1.5 µm step size. The raw EBSD patterns were recorded in NORDIF acquisition software and indexed offline in TSL OIM Data collection (Ametek, USA) with body centred cubic (BCC) tantalum as a possible crystal structure. After that the EBSD maps were built in TSL OIM Analysis (Ametek, USA) software.

C. Result and Discussion

Crater profile Optimization

Since the most important aspects of crater profile evolution with various discharge parameters is already introduced, further details can be found in articles as referred.[14, 15, 23] It is worth mentioning that there are two typical operation modes for Astrum:- (i) to fix current and adjust gas flow to obtain desired voltage, termed as constant current mode; (ii) to fix voltage and adjust gas flow to obtain desired current, termed as constant voltage mode. Nevertheless, according to the authors' experience, the former approach was found to be more appropriate.[24] Therefore, constant current mode was used to obtain flat crater profiles in this work. Some examples of flat crater profiles obtained for control samples are shown in Figure 1. In order to get flat craters at higher currents also an increase of the gas flow is needed. The gas flow rates are expressed in standard cubic centimetre per minute (sccm) or equivalent unit, millilitre per minute (ml/min). It is observed that for lower voltages (0.6-0.8 kV), a voltage to current ratio of ~0.3 (kV/mA) leads to flat craters, while for higher voltages (0.9-1 kV) the necessary ratio drops to ~0.2 (kV/mA). The voltage to current ratio in range of 0.2-0.35 (kV/mA) is slightly below the flat crater conditions for copper where the ratio is 0.3-0.4 (kV/mA).[22] The slight deviation might be related to a different matrix type introducing changes in the material properties for example, the secondary emission coefficient and thermal conductivity of the cathode material. Similar work on silicon resulted into flat crater at discharge condition of 2.3 mA and 0.7 kV. Crater profiles together with other results on silicon will be covered in another paper. It is possible that same conditions may not exactly fit for other matrices but can certainly serve as a starting point for crater shape optimization. In case flat craters are not obtained, it is recommended to fix one among current or voltage and change the other parameter as demonstrated in ref. 15.

The classical Boumans' equation describes a linear relationship of sputtering rate with voltage.[25] Indeed, a linear correspondence between sputtering rate and voltage is observed when current is kept constant at 3 mA (Figure S1). Additionally, if the Boumans' equation is applied to the present data, the threshold voltage (V_0) is about ~0.23 kV, which is reasonably close to the value reported for tantalum in Boumans' article (V_0 = 0.32 kV). To be mentioned, it is still possible to obtain a flat crater below 0.6 kV. However, when the GD voltage is too low approaching the threshold potential, then the plasma becomes less stable. In addition, keeping an optimal ratio (0.2-0.35 kV/mA) for obtaining flat craters would require a very low current. As a consequence, the matrix signal intensity would be reduced, i.e. the measurement sensitivity will have to be compromised. Likewise, for higher voltages above 1 kV, current supply above 5 mA is needed. In our experience, there is higher fluctuation in current and/or voltage at such high values of the parameters and therefore such conditions are not recommended.

It should be brought into attention that while performing weight loss experiments, weight of the sample before and after sputtering at a particular discharge condition is needed. This requires use of sensitive analytical balance that can accurately measure the difference in weight. For this work, analytical balance (PA224C, OHAUS Pioneer, Switzerland) was used that allows readability up to 0.1 mg. Therefore, to facilitate the variation in weight loss, use of higher current is advised. In this work, current of 3 mA was used to sputter tantalum sample with small grains for 30 minutes at various voltages in range of 0.6- 1.9 kV (Figure S1).

Differential sputtering

After sputtering the test sample for 1.5 h at a discharge condition of 5 mA and 1 kV using argon flow of 0.55 ml/min, the grains inside the crater were visible with naked eyes. The corresponding crater profile is presented in Figure 2. As observed, there is a clear 'step' in the crater profile, which indicates differential sputtering. To check if the observed step persists, the sample was re-inserted to the instrument and sputtered at the same spot for another 1

h (total 2.5 h) using same discharge condition (5 mA, 1 kV). This time using argon flow of 0.43 ml/min. The setting up of the sample into the sample holder and insertion of sample probe into GD chamber is a manual process. Despite of being mindful of this fact, an adjustment of argon flow from initial value of 0.55 ml/min to 0.43 ml/min was needed to obtain the same discharge condition (5 mA, 1 kV). This is probably linked to the change in crater bottom roughness as compared to freshly polished surface when sputtered initially. However, interestingly, the variation in gas flow rates did not alter the crater shape from initially obtained flat crater bottom (Figure 2 and 3).

The accompanying scanning electron micrograph image of the crater after 2.5 h (1.5 h+1 h sputtering) is presented in Figure 3A. The vertical- and horizontal lines indicate locations where two crater profiles were measured. The profile along the horizontal line was measured twice, once after 1.5 h of sputtering (Figure 2) and the second time after additional 1 h sputtering (Figure 3B). The profile measured along the vertical line (after 1.5 h+1 h sputtering) is crossing three grains. Two well developed steps (Figure 3C) are clearly visible along the bottom of the crater. Therefore, EBSD was performed inside the actual crater to check whether the steps corresponded to different grain orientations, i.e. grain boundaries. The results obtained are presented in Figure 4 as secondary electron micrograph (Figure 4A) and corresponding inverse pole figure (Figure 4B). Indeed, the inverse pole figure indicates that three different grain orientation exists. The correlation between the EBSD map and profilometer map showed that the grain close to plane orientation (111) sputters less as compared to a grain that is in between planes (001) and (101) (Figure 3B and 4). Also, the grain close to plane (101) sputters almost equally to the grain being in between planes (001) and (101) (Figure 3C and 4). This observation is consistent and can be verified further through Figure S2, where the blue grain with (111) plane is at a different height compared to the other two planes. It should be mentioned, however, that other studies exist, stating presence of differential sputtering as a function of crystallographic orientation when the energy of probing ions are above 1 keV.[26-28] Interestingly, differential sputtering can also be observed in GDMS where ion energies are at or lower than 1 keV.[29]

Also, it was checked whether differential sputtering is occurring with large grains when lower voltage and current were used. Here, the observation of the step is consistent at 3 mA, 0.8 kV (at 0.28 ml/min argon flow) and 2.3 mA, 0.7 kV (at 0.37 ml/min argon flow) each after 2 h of sputtering (Figure 5). The grain texture difference could potentially be the reason for variation in argon flow rates in order to obtain flat crater using the same discharge condition (2.3 mA, 0.7 kV) for the control sample (Figure 1B) and the test sample (Figure 5B). In Figure 5, the depth axis scale is changed (zoomed) from what is used in Figure 2 and 3 to show the presence of steps. It has to be pointed out that accurate quantitative value to estimate the differential sputtering or roughness is not presented in this paper. The grain texture varies from one sample to another. Also, for polycrystalline material it is likely that the roughness at the crater bottom is always changing. Thus, it is challenging to provide accurate quantitative data about differential sputtering and roughness for polycrystalline material. Also, ideally the EBSD map of entire crater is required to precisely identify the grain orientations to comment on its contribution to differential sputtering and roughness. Such limitations or inadequacies of data representation does not deviate from the conclusion that differential sputtering is present for the samples used in this study. Lines at the top and bottom of crater profile are used to indicate differential sputtering and roughness, where appropriate, to guide the reader.

There are probably several possible explanations to the observed differences in sputtering rates with different grain orientation. One plausible explanation can be linked to the variation in planar densities of the grains. Since plane (111) has lower density than (101), there could be slightly less energy and momentum transfer from the argon ions as they probe this plane. Conversely, higher momentum and energy transfer can be expected for denser planes. Zhang et al. performed similar work on tantalum with magnetron sputtering where (110) grains had higher sputtering rate as compared to (111) planes.[30] In another study performed by Chen et al. using GDOES on iron, sputtered depth for crystallites with different orientation were reported to be unequal.[23] Iron has also a BCC crystal structure and the authors reported less sputtering of (111)- than (001) planes.[23] In the present work the plane orientation showing the highest sputtering rate is in between the (001) and (101), and would have a planar density relatively close to (101). Hence, this is probably the reason why these planes sputter equivalently (Figure 3C and S2).

Roughness at crater bottom for materials with small grains

The entire study is designed using tantalum samples with different microstructure i.e. larger and smaller than 1 mm grain size so that only a few or many grains could be obtained within the crater. This allowed observation of results where effect of grains could be clearly demonstrated. There could be other reasons for crater bottom roughness. To mention a few- uneven sample polishing, presence of inclusions and other sub-grain structures. In fact, the sputtering process itself can lead to indentations as a result of argon ions hitting on sample surface which

contributes to some roughness. This is dependent on energy of the ion projectile hitting the sample surface which is also true for single crystals (monocrystalline) materials.[31] However, for samples used in present study, the effect of grains are likely to dominate. For tantalum with finer grains, where grain orientations differ substantially (Figure 6), a differential sputtering led to enhanced crater bottom roughness (Figure 1D and 7) as compared to tantalum with large grains (Figure 2-4 and S2), when both types of tantalum were sputtered at same discharge condition (5 mA, 1 kV). To compare if this observation is consistent with lower discharge condition, Figure 1B is replotted in Figure S3 with axis scale matching the axis scale in Figure 5B. The enhanced roughness is evident for the control sample (finer grains) as compared to the test sample (larger grains) when operated at same discharge condition of 2.3 mA, 0.7 kV (Figure 5B and Figure S3).

For polycrystalline material, therefore roughness can be fully or partially linked to differential sputtering of grains with different crystallographic orientations. It could likely be the reason why GDMS users almost always observe some roughness at the crater bottom. It is worth mentioning that according to some authors, atoms may have different sputter yields.[32] This phenomenon could eventually contribute to roughness if the concentration of impurities is high and the actual elemental sputter yields would be substantially different. However, for pure tantalum samples, major impurities are molybdenum, tungsten and niobium. All those elements do have similar sputtering yields. Hence, it is unlikely these impurities would contribute significantly to roughness of sputtered tantalum. Thus, at least for tantalum, the contribution of such an effect can be regarded negligible.

D. Conclusions

This study describes the impact of discharge parameters on crater profile optimization of tantalum. The voltage to current ratio in the range of 0.2-0.35 (kV/mA) resulted into flat craters. Thus, flat craters were obtained for five different discharge settings: - (i) 2 mA, 0.6 kV; (ii) 2.3 mA, 0.7 kV; (iii) 3 mA, 0.8 kV; (iv) 4 mA, 0.9 kV and (v) 5 mA, 1 kV. It is likely that the differential sputtering of grains has a dominating contribution to the cater bottom roughness in the studied samples. However, more investigations of various materials with larger and smaller grains are needed to generalize this conclusion.

Conflicts of interest

The authors have no conflicts to declare.

Acknowledgements

The authors are thankful to Nu Instruments scientist, Dr Benoit Disch for providing tantalum sample and for fruitful discussions regarding crater shape optimization.

Notes and references

[a] Department of Materials Science and Engineering, Norwegian University of Science and Technology, 7491 Trondheim, Norway.
[b] MK2 Technologies Inc., Jamesville NY 13078, USA
**Corresponding author: gagan.paudel@ntnu.no*

1. A. Bogaerts, E. Neyts, R. Gijbels and J. van der Mullen, *Spectrochimica Acta Part B: Atomic Spectroscopy*, 2002, **57**, 609-658.
2. R. K. Marcus and J. Broekaert A. C., *Glow Discharge Plasmas in Analytical Spectroscopy* John Wiley & Sons Ltd, 2003.
3. C. Venzago and J. Pisonero, in *Sector Field Mass Spectrometry for Elemental and Isotopic Analysis*, The Royal Society of Chemistry, 2015, DOI: 10.1039/9781849735407-00319, pp. 319-380.
4. A. A. Ganeev, A. R. Gubal, K. N. Uskov and S. V. Potapov, *Russian Chemical Bulletin*, 2012, **61**, 752-767.
5. J. Pisonero, J. Fandino, J. H. Nordlien, S. Richter, J. Pfeifer, C. D. Quarles, J. Gonzalez, N. Jakubowski and N. Bordel, *Journal of Analytical Atomic Spectrometry*, 2019, **34**, 2252-2260.
6. J. Pisonero, B. Fernández, R. Pereiro, N. Bordel and A. Sanz-Medel, *TrAC Trends in Analytical Chemistry*, 2006, **25**, 11-18.
7. P. Konarski, K. Kaczorek, M. Ćwil and J. Marks, *Vacuum*, 2008, **82**, 1133-1136.
8. J. Pisonero, R. Valledor, A. Licciardello, C. Quirós, J. I. Martín, A. Sanz-Medel and N. Bordel, *Analytical and Bioanalytical Chemistry*, 2012, **403**, 2437-2448.
9. J. Pisonero, B. Fernández and D. Günther, *Journal of Analytical Atomic Spectrometry*, 2009, **24**, 1145-1160.

10. R. Payling, D. Jones and A. Bengtson, *Glow Discharge Optical Emission Spectrometry*, Wiley, 1997.
11. L. Lobo, B. Fernández and R. Pereiro, *Journal of Analytical Atomic Spectrometry*, 2017, **32**, 920-930.
12. M. Di Sabatino, C. Modanese and L. Arnberg, *Journal of Analytical Atomic Spectrometry*, 2014, **29**, 2072-2077.
13. C. Modanese, G. Gaspar, L. Arnberg and M. Di Sabatino, *Analytical and Bioanalytical Chemistry*, 2014, **406**, 7455-7462.
14. A. Bogaerts and R. Gijbels, *Spectrochimica Acta Part B: Atomic Spectroscopy*, 1997, **52**, 765-777.
15. A. Bogaerts, W. Verscharen and E. Steers, *Spectrochimica Acta Part B: Atomic Spectroscopy*, 2004, **59**, 1403-1411.
16. J. Pisonero, I. Feldmann, N. Bordel, A. Sanz-Medel and N. Jakubowski, *Analytical and Bioanalytical Chemistry*, 2005, **382**, 1965-1974.
17. D. Demény, L. Szücs and M. Adamik, *Journal of Analytical Atomic Spectrometry*, 1992, **7**, 707-710.
18. L. Wilken, V. Hoffmann and K. Wetzig, *Journal of Analytical Atomic Spectrometry*, 2003, **18**, 1133-1140.
19. G. J. M. Hagelaar and L. C. Pitchford, *Journal of Analytical Atomic Spectrometry*, 2002, **17**, 1408-1410.
20. N. P. Ferreira and P. A. Büger, *Redeposition of Sputtered Material in a Glow-Discharge Lamp Measured by Means of an Ion Microprobe Mass Analyser*, Report 18657109, National Physical Research Laboratory, Pretoria, South Africa, 1978.
21. A. Raith, R. C. Hutton and J. C. Huneke, *Journal of Analytical Atomic Spectrometry*, 1993, **8**, 867-873.
22. B. Disch, presented in part at the International Glow Discharge Spectroscopy Symposium, IGDSS2018, Berlin, Germany, 2018.
23. L. Chen, M. C. Simmonds, S. Habesch and J. M. Rodenburg, *Surface and Interface Analysis*, 2001, **31**, 206-211.
24. G. Paudel, M. Kasik and M. Di Sabatino, *Journal of Analytical Atomic Spectrometry*, 2019, **34**, 1829-1837.
25. P. W. J. M. Boumans, *Analytical Chemistry*, 1972, **44**, 1219-1228.
26. G. D. Magnuson and C. E. Carlston, *J Appl Phys*, 1963, **34**, 3267-3273.
27. A. L. Southern, W. R. Willis and M. T. Robinson, *J Appl Phys*, 1963, **34**, 153-163.
28. R. Behrisch and W. Eckstein, *Sputtering by Particle Bombardment*, Springer, 2007.
29. A. Bogaerts, PhD, University of Antwerp, 1996.
30. Z. Zhang, L. Kho and C. E. W. Jr., *J Vac Sci Technol A*, 2006, **24**, 1107-1111.
31. D. Moreno and D. Eliezer, *Journal of Materials Science Letters*, 1994, **13**, 1591-1593.
32. R. K. Marcus, *Glow Discharge Spectroscopies*, Springer Science, 1991.

Figures

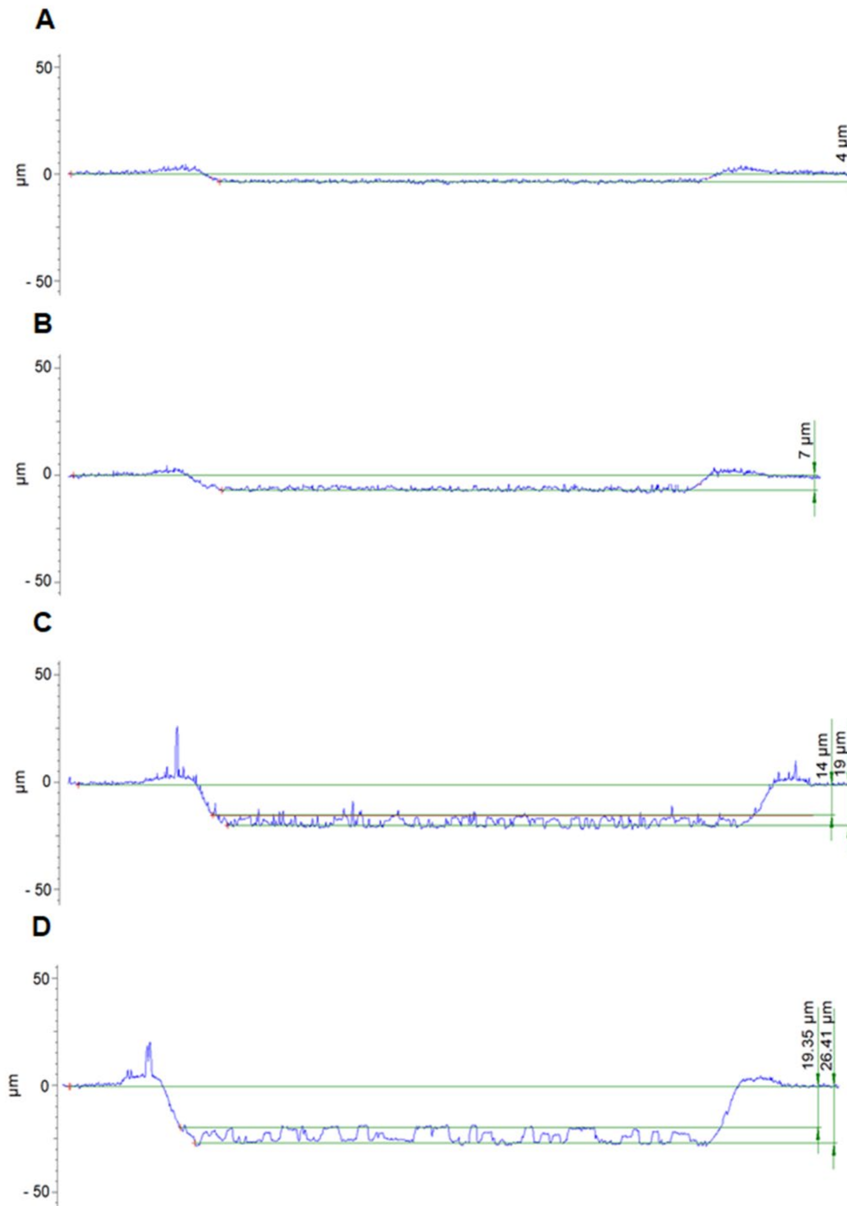

Figure 1: Flat crater profile optimized for tantalum with small grains at various discharge conditions of 2 mA, 0.6 kV using 0.27 ml/min argon flow (A); 2.3 mA, 0.7 kV using 0.25 ml/min argon flow (B); 4 mA, 0.9 kV using 0.30 ml/min using argon flow (C); and 5 mA, 1 kV using 0.41 ml/min argon flow (D), each after sputtering for 1.5 h.

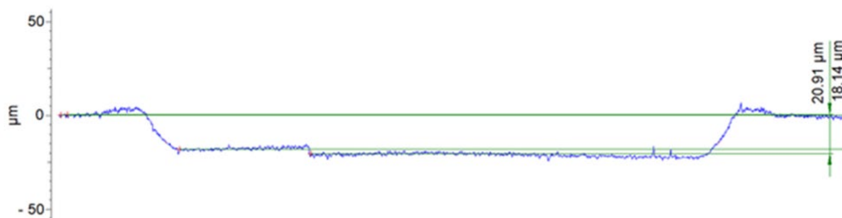

Figure 2: Crater profile of tantalum with large grains after 1.5 h of sputtering at discharge condition of 5 mA, 1 kV using 0.55 ml/min argon flow.

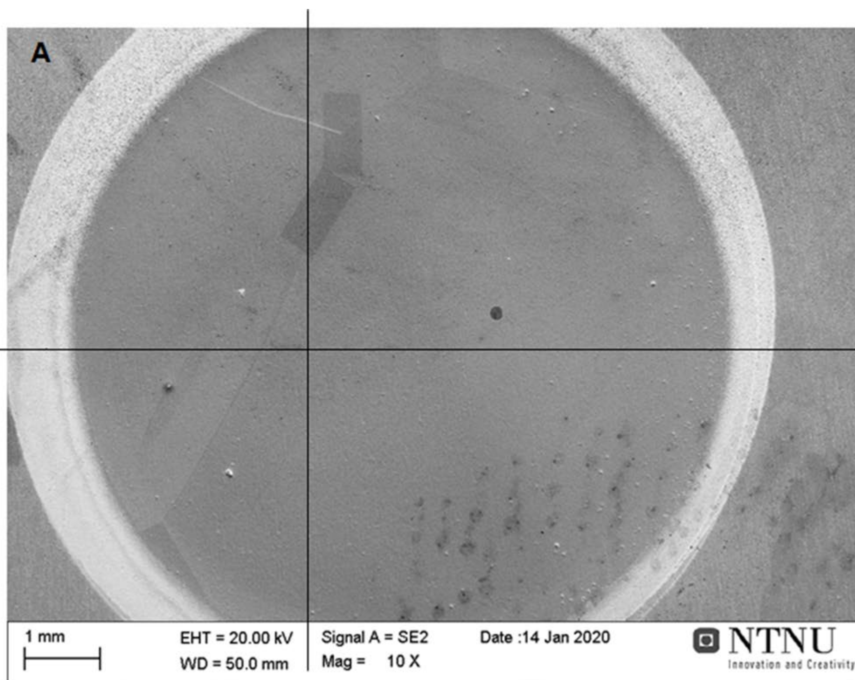

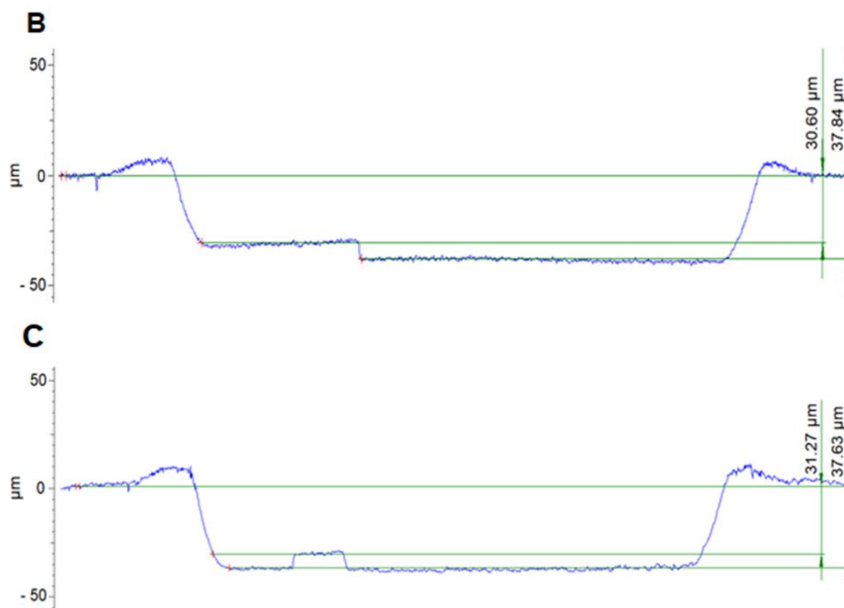

Figure 3: Scanning electron micrograph of tantalum with large grains after additional 1 h of sputtering (total 2.5 h sputtering) at discharge condition of 5 mA, 1 kV using 0.43 ml/min argon flow (A), the corresponding crater profile map upon horizontal (B) and vertical (C) measurement along the line using a mechanical profilometer.

A

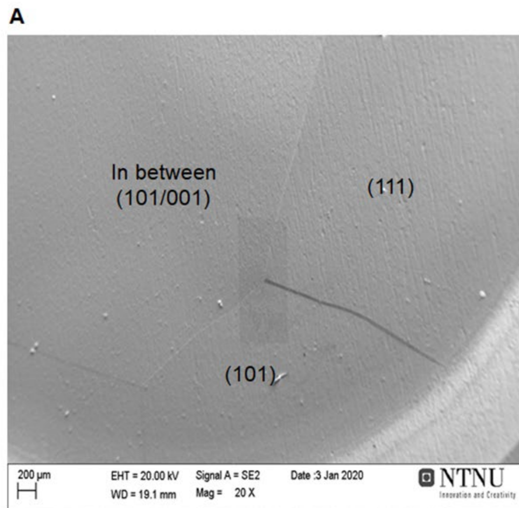

B

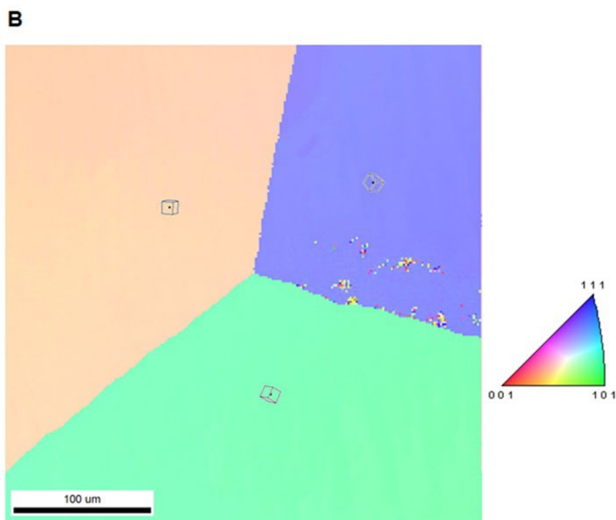

Figure 4: Scanning electron micrograph of tantalum with large grains showing shaded region where electron backscattered diffraction was performed (A), and corresponding inverse pole figure (B) after 2.5 h sputtering at discharge condition of 5 mA, 1 kV. Corresponding inverse pole figure legend to the right.

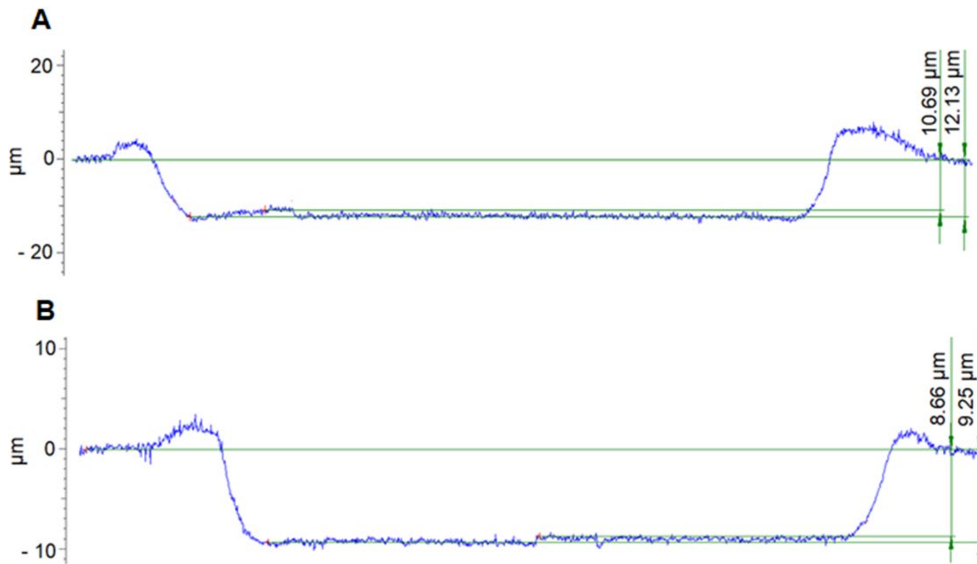

Figure 5: Crater profiles for tantalum with large grains at various discharge conditions of 3 mA, 0.8 kV using 0.28 ml/min argon flow (A), and 2.3 mA, 0.7 kV using 0.37 ml/min (B), each after 2 h of sputtering.

Figure 6: EBSD map for tantalum with small grains at discharge conditions of 5 mA, 1 kV using 0.41 ml/min argon flow after sputtering for 1.5 h. Corresponding inverse pole figure legend to the right.

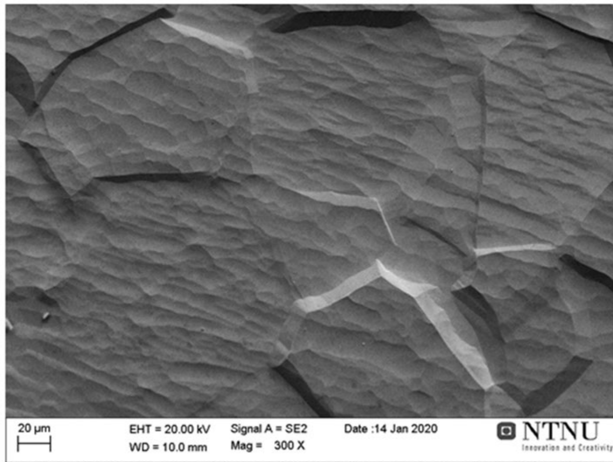

Figure 7: Scanning electron micrographs of tantalum with smalls grains at discharge conditions of 5 mA, 1 kV using 0.41 ml/min argon flow after sputtering for 1.5 h.

Supplementary Information

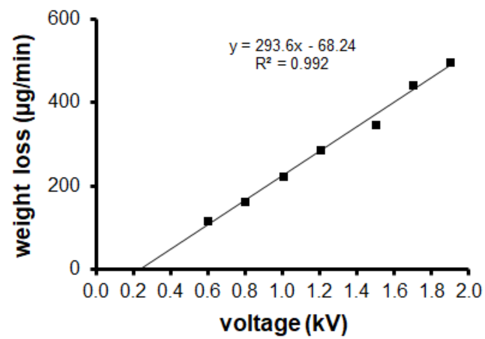

Figure S1: Relationship between sputtering rate in terms of weight loss and voltage for tantalum with small grains.

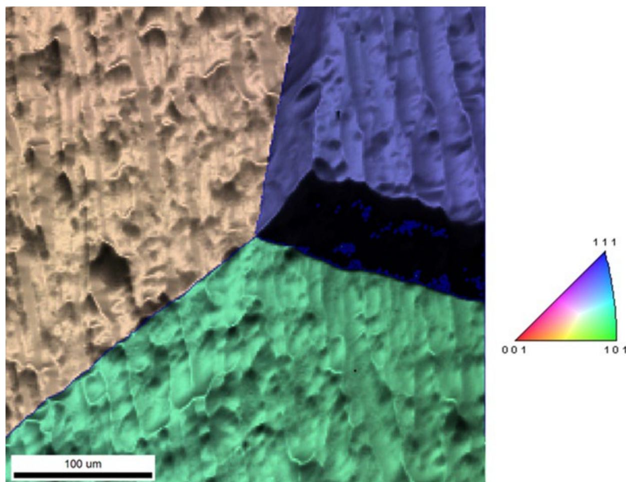

Figure S2: EBSD map overlaid over secondary electron micrograph for tantalum sample with large grains showing grain boundaries and differential sputtering after 2.5 h sputtering at discharge condition of 5 mA, 1 kV. Corresponding inverse pole figure legend to the right.

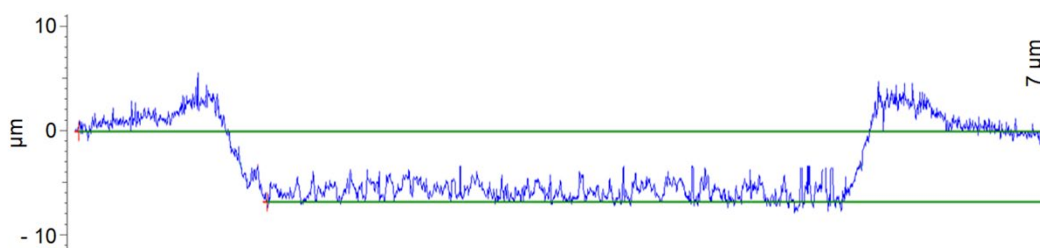

Figure S3: Flat crater profile for tantalum with small grains at discharge condition of 2.3 mA, 0.7 kV using 0.25 ml/min argon flow after sputtering for 1.5 h, zoomed with a different axis scale using Figure 1B.